BIOCHEMISTRY
including biophysical chemistry & molecular biology

Article

pubs.acs.org/biochemistry

Structural Basis for the Divergence of Substrate Specificity and Biological Function within HAD Phosphatases in Lipopolysaccharide and Sialic Acid Biosynthesis

Kelly D. Daughtry,[†] Hua Huang,[‡] Vladimir Malashkevich,[§] Yury Patskovsky,[§] Weifeng Liu,[§] Udupi Ramagopal,[§] J. Michael Sauder,[∥] Stephen K. Burley,[∥,#] Steven C. Almo,[§] Debra Dunaway-Mariano,*[,‡] and Karen N. Allen*[,⊥]

[†]Department of Physiology and Biophysics, Boston University School of Medicine, Boston, Massachusetts 02118-2394, United States
[‡]Department of Chemistry and Chemical Biology, University of New Mexico, Albuquerque, New Mexico 87131-0001, United States
[§]Department of Medicine, Albert Einstein College of Medicine, Bronx, New York 10461, United States
[∥]Lilly Biotechnology Center, 10300 Campus Point Drive, San Diego, California 92121, United States
[⊥]Department of Chemistry, Boston University, Boston, Massachusetts 02215-2521, United States

Supporting Information

ABSTRACT: The haloacid dehalogenase enzyme superfamily (HADSF) is largely composed of phosphatases that have been particularly successful at adaptating to novel biological functions relative to members of other phosphatase families. Herein, we examine the structural basis for the divergence of function in two bacterial homologues: 2-keto-3-deoxy-D-manno-octulosonate 8-phosphate phosphohydrolase (KDO8P phosphatase, KDO8PP) and 2-keto-3-deoxy-9-O-phosphononononic acid phosphohydrolase (KDN9P phosphatase, KDN9PP). KDO8PP and KDN9PP catalyze the final step in KDO and KDN synthesis, respectively, prior to transfer to CMP to form the activated sugar nucleotide. KDO8PP and KDN9PP orthologs derived from an evolutionarily diverse collection of bacterial species were subjected to steady-state kinetic analysis to determine their specificities toward catalyzed KDO8P and KDN9P hydrolysis. Although each enzyme was more active with its biological substrate, the degree of selectivity (as defined by the ratio of k_{cat}/K_m for KDO8P vs KDN9P) varied significantly. High-resolution X-ray structure determination of *Haemophilus influenzae* KDO8PP bound to KDO/VO_3^- and *Bacteriodes thetaiotaomicron* KDN9PP bound to KDN/VO_3^- revealed the substrate-binding residues. The structures of the KDO8PP and KDN9PP orthologs were also determined to reveal the differences in their active-site structures that underlie the variation in substrate preference. Bioinformatic analysis was carried out to define the sequence divergence among KDN9PP and KDO8PP orthologs. The KDN9PP orthologs were found to exist as single-domain proteins or fused with the pathway nucleotidyl transferases; the fusion of KDO8PP with the transferase is rare. The KDO8PP and KDN9PP orthologs share a stringently conserved Arg residue that forms a salt bridge with the substrate carboxylate group. The split of the KDN9PP lineage from the KDO8PP orthologs is easily tracked by the acquisition of a Glu/Lys pair that supports KDN9P binding. Moreover, independently evolved lineages of KDO8PP orthologs exist, and are separated by diffuse active-site sequence boundaries. We infer a high tolerance of the KDO8PP catalytic platform to amino acid replacements that in turn influence substrate specificity changes and thereby facilitate the divergence in biological function.

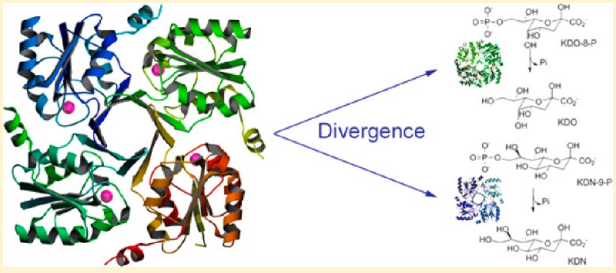

The haloacid dehalogenase enzyme superfamily (HADSF) has proven to be an excellent system for examining the structural basis for the divergence in function among paired homologues within a common evolutionary clade.[1−3] Hallmarks of this superfamily include its large size (>83,000 members to date in Pfam), high degree of sequence diversity, and broad substrate range.[4] At the top of the HADSF hierarchy, the phosphatases (which compose >99% of the family)[5] are divided into broad structural classes (C0, C1, C2A, and C2B)[4,6] on the basis of the location (relative to the catalytic motifs), size (extended loops vs inserted domain (termed the cap domain)), and topology of the loops/domain inserts to the highly conserved Rossmann-fold catalytic domain (termed the core domain). In turn, the individual structural classes are composed of clades,[4] of which the members are closely related in structure and evolutionary history yet perform unique biological functions. Our goal is to gain insight into the process of

Received: May 26, 2013
Revised: July 11, 2013
Published: July 12, 2013

functional change within these distinct lineages of HADSF phosphatases.

In the present study, we targeted a lineage of sequences within the "YbrI" clade of the type-C0 structural class (the typical structure is shown in Figure 1A,B).[4] The biological unit is comprised of four identical Rossmann-fold subunits that oligomerize via a central β-barrel formed from the respective four β-loop-β inserts (colored yellow in Figure 1A,B). The active site is formed at the interface of two adjacent subunits, and there are four active sites per tetramer in total. The catalytic scaffold, located at the C-terminal end of the Rossmann central parallel β-sheet, contains catalytic motifs 1−4 (colored red, green, cyan, and orange, respectively) and the bound Mg^{2+} cofactor (magenta sphere). The residues located on the adjacent subunit (known as the cap subunit, which is analogous to the cap domain) complete the active site (Figure 1B).

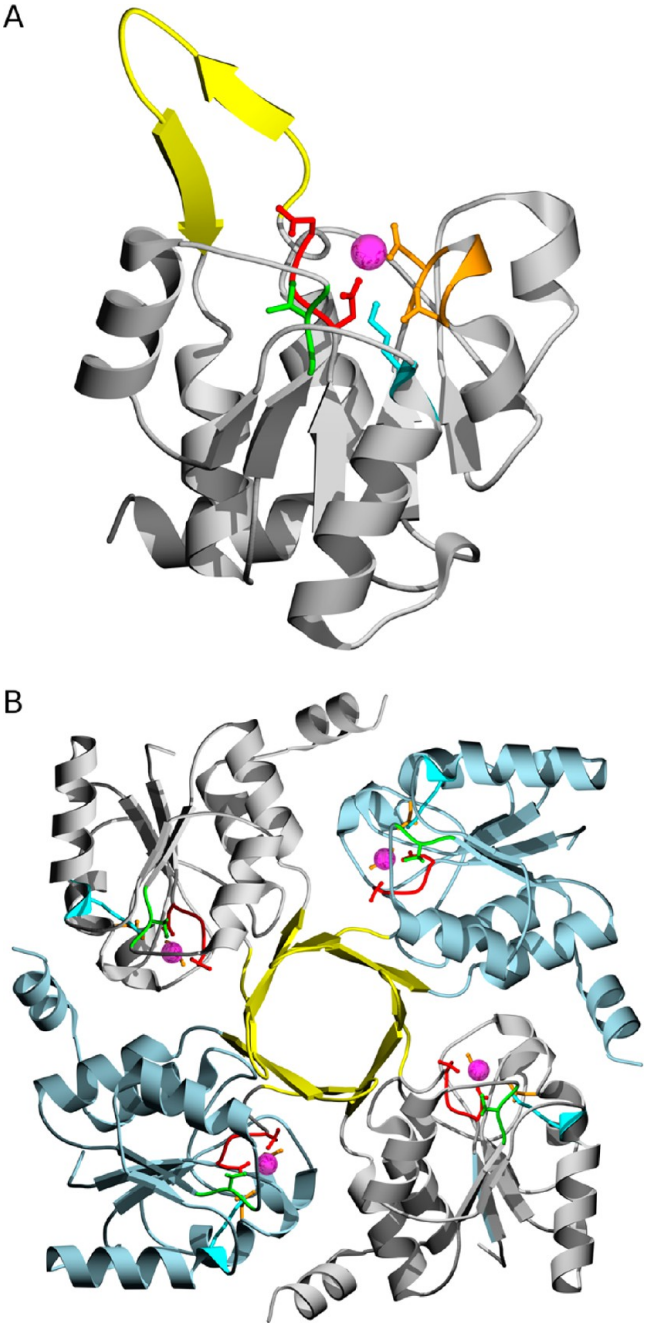

Figure 1. KD9PP monomer (A) and tetramer (B) structures (PDB ID 3E8M). The HADSF Rossmann-fold domain is colored gray or light blue, with the tetramerization flap colored yellow. The HADSF catalytic motifs are colored red (motif 1), green (motif 2), cyan (motif 3), and orange (motif 4), and the magnesium cofactor is shown in magenta. This figure and all others unless indicated were generated with MOLSCRIPT[41] and POVscript+.[42]

The two enzyme activities attributed to the YbrI clade are those of the 2-keto-3-deoxy-D-manno-octulosonate 8-phosphate (KDO8P) phosphatase (KDO8PP)[7,8] and 2-keto-3-deoxy-D-glycero-D-galacto-nonic acid-9-phosphate (KDN9P) phosphatase (KDN9PP).[9] The structures of the α- and β-anomers of KDO8P and KDN9P are illustrated in Chart 1. KDO is a saccharide integral to lipid A in Gram-negative bacteria and is critical for survival.[10−14] KDN is a nine-carbon sialic acid derivative commonly used in cell-wall polysaccharides in higher level organisms, which unexpectedly has also appeared in bacteria.[15] KDO8PP and KDN9PP catalyze the final step in the synthesis of KDO and KDN, which are subsequently activated with a C(1) cytosine monophosphate (CMP) group (Scheme 1). The means of conferring specificity for KDO8PP and KDN9PP is not clear from primary-sequence alignments or from the examination of the available liganded structures.[9,16]

The goals of this work were to define the structural basis for the divergence in substrate preference among homologues, the relationship between substrate preference and biological function, and the evolutionary pathways that determine structure and function. Steady-state kinetic constants that define substrate preference (KDO8P vs KDN9P) of targeted YrbI-clade phosphatases were determined. Next, we examined the KDO8PP and KDN9PP X-ray structures, which revealed the substrate-binding motifs responsible for discriminating between KDO8P and KDN9P. The substrate-specificity residues thus defined were used in combination with gene context analysis to identify KDO8PP and KDN9PP orthologs among homologous sequences. On the basis of the examination of these data, the biological ranges of KDO8PP and KDN9PP were determined, and alignments of the ortholog sequences, grouped according to KDO8PP and KDN9PP structural classes, were used to generate an unrooted phylogenetic tree that provides insight into the evolutionary history of KDO8PP and KDN9PP. Finally, we propose a model for the divergence of the structure and substrate preference that accompanies the adaptation of the YbrI-clade scaffold to perform one of two distinct biological functions (KDO vs KDN synthesis).

MATERIALS AND METHODS

Materials, Cloning, and Site-Directed Mutagenesis. Unless otherwise stated all chemicals were obtained from Sigma-Aldrich, and all primers, competent cells, ligases, polymerases, and restriction enzymes were from Invitrogen. The gene encoding BT1713 (BT-KDN9PP) was previously cloned.[17] The plasmid containing the coding sequence for HI1679 (HI-KDO8PP) from *Haemophilus influenzae* was a generous gift from Dr. Osnat Herzberg at the Center for Advanced Research in Biotechnology, University of Maryland Biotechnology Institute, Rockville, Maryland. The gene encoding BT1677 (BT-KDO8PP) was amplified from *Bacteriodes thetaiotaomicron* VPI-5482 genomic DNA with primers 5′-CCGGCGGGGAGAATTGGAGGCTAATATAA-3′ (forward) and 5′-GCTGGCAGACAGTCAGGCATTGCAGGAAAT-3′ (reverse). After amplification, the clone was modified to

dx.doi.org/10.1021/bi400659k | *Biochemistry* 2013, 52, 5372−5386

Chart 1

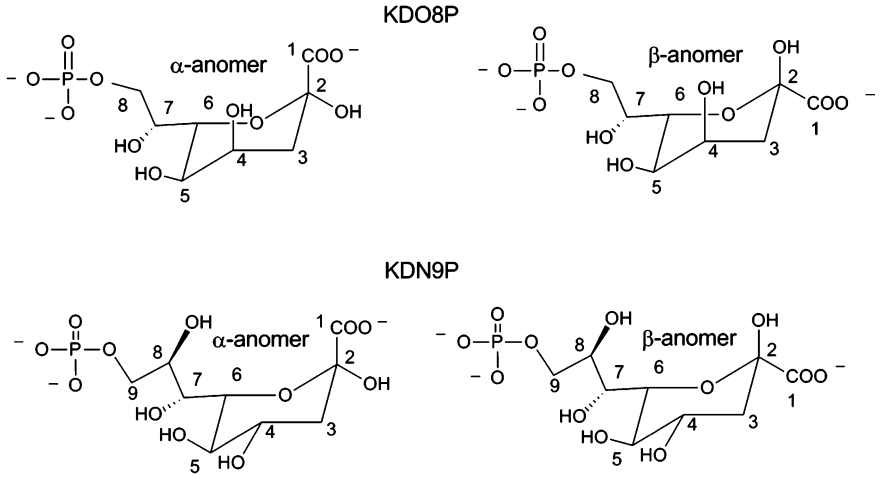

Scheme 1. Biosynthetic Pathways Leading to the Cytidine Monophosphate (CMP)-Substituted β-Anomers of KDO and KDN

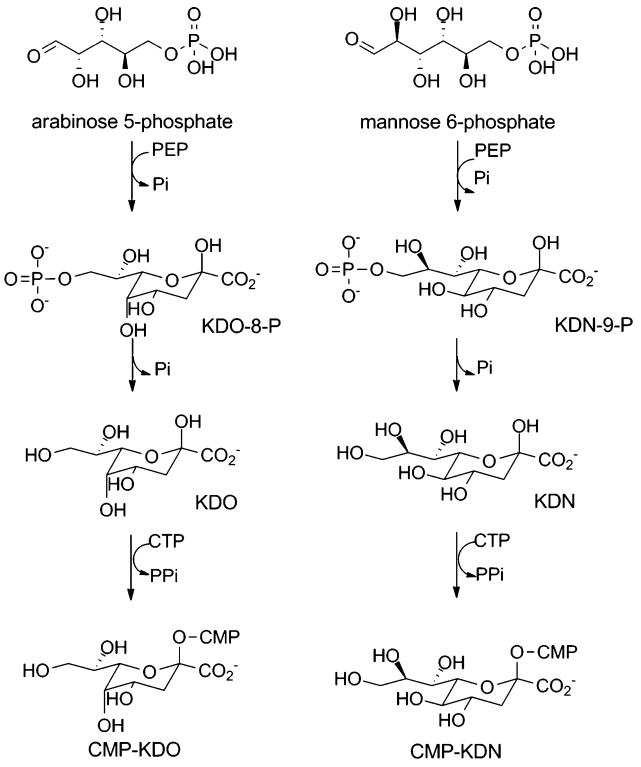

include the restriction sites for NdeI and BamHI using primers 5′-GTAAAAG**CATATG**AGCACCATCAATTATGATTATCCCGC-3′ (NdeI) and 5′-TTATTAAAG**GGATCC**ACAACTCACCAGCCGAAAGCATCTTCCGCC-3′ (BamHI) (bold letters indicate the restriction sites). After amplification, the clone was digested with NdeI and BamHI. The fragment was cloned into a pET15b vector containing an N-terminal His_6-tag and thrombin cleavage site.

BT-KDN9PP and BT-KDO8PP genes bearing site-directed mutations were prepared using a PCR-based strategy with primers encoding the desired codon change and native flanking sequence and the wild-type BT-KDN9PP or BT-KDO8PP plasmid serving as the template. The gene sequence was confirmed by DNA sequencing (University of New Mexico sequencing facility).

Expression and Purification. Recombinant BT-KDN9PP (wild-type and mutants) and HI-KDO8PP were expressed and purified as previously described.[7,17] Recombinant BT-KDO8PP was purified from *Escherichia coli* BL-21(DE3) cells transformed with the pET15b vector harboring the BT-KDO8PP sequence. The cells were grown in LB media at 37 °C until A_{600} = 1.0, at which point IPTG was added to a final concentration of 1 mM. The cells were harvested by centrifugation (7800*g*) after 4 h. The cell pellets were suspended in 20 mM HEPES (pH 7.5) and 100 mM NaCl and lysed by sonication. The cell debris was removed by centrifugation (48 400*g*) for 45 min. The supernatant was filtered using a 0.22 μm sterile filter and applied to a TALON Metal Affinity Resin (Clontech) gravity column (5 mL) equilibrated in 20 mM HEPES pH (7.5), 100 mM NaCl, and 10 mM imidazole. BT-KDO8PP was eluted using a step gradient of imidazole (30 mM, 100 mM, 250 mM, and 500 mM). The fractions containing BT-KDO8PP were analyzed by SDS-PAGE, pooled, and dialyzed against 2 L of 20 mM HEPES (pH 7.5), 100 mM NaCl, 10 mM imidazole, and 1 mM DTT. The dialyzed protein was cleaved by incubating with Tagzyme DAPase (Qiagen) for 2 h at 37 °C with shaking (250 rpm). The cleavage mixture was applied to the TALON Metal Affinity Resin (Clontech) gravity column (5 mL) pre-equilibrated in 20 mM HEPES (pH 7.5), 100 mM NaCl, and 10 mM imidazole. The flow through was analyzed by SDS-PAGE, pooled, and dialyzed against 2 L of 20 mM HEPES buffer (pH 7.5), 50 mM NaCl, and 10 mM $MgCl_2$. The purified protein was concentrated to 30 mg/mL using an Amicon Ultra Concentrator. Typical yields were 3.8 mg of protein/g of cell paste. The protein was >90% pure as assessed by SDS/PAGE analysis.

Crystallization, Data Collection, and Structure Solution of BT-KDO8PP. Crystals of BT-KDO8PP were obtained by the vapor-diffusion method using hanging-drop geometry. The drops were equilibrated against a reservoir solution containing 30% poly(ethylene glycol) (PEG) MME 550, 40 mM $MgCl_2$, and 100 mM HEPES (pH 7.5) at 18 °C. The hanging drops contained equal volumes (1 μL each) of the reservoir solution and a 30 mg/mL protein solution in 20 mM HEPES (pH 7.5), 50 mM NaCl, and 10 mM $MgCl_2$. Small crystals (0.1 × 0.1 × 0.05 mm^3) appeared within 2 d. The crystals belonged to the space group $P2_12_12_1$, with four

dx.doi.org/10.1021/bi400659k | *Biochemistry* 2013, 52, 5372−5386

protomers in the asymmetric unit and solvent composing 35% of the unit cell. Surface solvent was removed using Paratone, and the resulting crystals were flash-cooled in liquid nitrogen. Data were collected at 100 K using a single wavelength (1.0 Å) at the X12C beamline of the National Synchrotron Light Source (Brookhaven National Laboratory, Upton, New York). For the data collection, beamline X12C was equipped with a Brandeis 2 × 2 CCD detector. The data were collected to a 1.8 Å resolution and processed with the DENZO and SCALEPACK programs.[18]

The structure of the wild-type BT-KDO8PP-Mg^{2+} complex was refined to a 1.8 Å resolution with phases determined by the molecular replacement method using the MOLREP program in the CCP4 suite.[19−21] The search model was the protomer of BT-KDN9PP (BT1713), leading to a clear solution for four protomers (forming the expected tetramer). The structure was refined using the PHENIX program[22] with data between 36.7 and 1.8 Å, for which $F \geq 2\sigma(F)$ with alternating cycles of positional- and individual-temperature-factor refinement. The resulting model was manually inspected and modified using the COOT program.[23] In the final stages of the refinement, water molecules were added to the model using an electron-density acceptance criteria of $d \geq 3\sigma(d)$ in the *Fo*−*Fc* difference electron-density map. Magnesium ions were added in the final stage of the refinement, with an electron-density acceptance criteria of $d \geq 5\sigma(d)$ in the *Fo*−*Fc* map. The specific unit-cell parameters, data collection, and refinement statistics are presented in Table 2. The final model consisted of the following residues: chain A, 2−166; chain B, 2−165; chain C, 2−166; and chain D, 2−166.

Crystallization, Data Collection, and Structure Solution of the BT-KDN9PP Complex with KDN/VO_3^-. The crystals of BT-KDN9PP were obtained by the vapor-diffusion method with hanging-drop geometry. The drops were equilibrated against a reservoir solution containing 19% PEG 3350 and 100 mM magnesium formate at room temperature. The hanging drops contained equal volumes (1 μL each) of the reservoir solution and a 29 mg/mL protein solution in 10 mM HEPES (pH 7.5) and 10 mM $MgCl_2$. Small crystals (0.15 × 0.15 × 0.01 mm^3) appeared in 1 d. The crystals were soaked in a 50 μL solution of 50 mM KDN (Sigma-Aldrich, no. 60714), 20 mM sodium vanadate (Na_3VO_4), 22% PEG 3350, and 100 mM magnesium formate for 1 week before data collection. The crystals belonged to the $P2_12_12$ space group. Surface solvent was removed by passing the crystal through paratone followed by flash-cooling it in liquid nitrogen. The data were collected at a single wavelength (1.54 Å) on the Bruker Microstar-H running at 2.7 kW with Helios multilayer optics and a Platinum 135 CCD detector at Bruker AXS, Madison, Wisconsin. The data were collected to 2.1 Å, reduced using SAINT, and scaled using SADABS from the PROTEUM2 software suite.[24]

The structure of ligand-bound BT-KDN9PP was determined by molecular replacement to a 2.1 Å resolution using the MOLREP program in the CCP4 suite[20] and the protomer of BT-KDN9PP as the search model. A clear solution for four protomers (the expected tetramer) was obtained. Successive rounds of model refinement were performed using the PHENIX program [22] with data between 50 and 2.1 Å, for which $F \geq 2\sigma(F)$ with alternating cycles of positional- and individual-temperature-factor refinement. The resulting model was inspected and modified using the COOT program. In the final stages of the refinement, water molecules were added to the model with electron-density acceptance criteria of $d \geq 3\sigma(d)$ in the *Fo*−*Fc* difference electron-density map. Ligands (KDN and VO_3^-) were added when the R_{free} was below 30%. A composite omit map with coefficients 2*Fo*−*Fc* was calculated using the CNS program. The unit-cell parameters, data collection, and refinement statistics are presented in Table 2. The final model showed density corresponding to VO_3^- at all four active sites and density corresponding to KDN at two of the active sites (Figure S12). Residue Gln164 in each chain (A, B, C, and D) was disordered and not modeled, as was Met1 of chain D.

The structures of the BT-KDN9PP-Glu56Ala and BT-KDN9PP-Glu56Ala/Lys67Ala variants bound to the Mg^{2+} cofactor were also solved. (See the Supporting Information for crystallization, data collection, and refinement details.)

Crystallization, Data Collection, and Structure Solution of HI-KDO8PP. The crystals of KDO8PP from *Haemophilus influenzae* (HI-KDO8PP) were obtained by the vapor-diffusion method with hanging-drop geometry. The drops were equilibrated at 17 °C against a reservoir solution containing 21% PEG 3550 and 100 mM Tris (pH 8.5). The hanging drops contained equal volumes (1 μL) of the reservoir solution and an 11 mg/mL solution of protein in 50 mM HEPES (pH 7.6), 5 mM $MgCl_2$ and 1 mM DTT. Small crystals (0.15 × 0.1 × 0.05 mm^3) appeared in within 1 d. The crystals were soaked in 50 μL of 100 mM Tris pH 8.5, 30% PEG 3350, 20 mM sodium vanadate, and 20 mM KDO (Sigma-Aldrich, no. K2755) for 3 d at room temperature before data collection. Surface solvent was removed by passing the crystal through Paratone followed by flash-cooling it in liquid nitrogen. The crystals belonged to the *I*4 space group. The data were collected at a single wavelength (1.54 Å) on a Bruker MICROSTAR microfocus rotating anode with Helios optics and Platinum 135 CCD detector using a four-circle kappa goniometer. The data were collected to a 1.8 Å resolution, reduced using SAINT, and scaled using SADABS from the PROTEUM2 software suite.[24]

The structure of ligand-bound HI-KDO8PP was determined to a 1.8 Å resolution with phases from the molecular replacement method using the MOLREP program in the CCP4 suite. The search model was the protomer of HI-KDO8PP (PDB ID: 1K1E, chain A with 7 C-terminal residues manually removed),[7] leading to a clear solution for a single protomer in the unit cell. The presence of twinning was confirmed by the examination of the cumulative intensity distribution, with a twinning fraction of 0.33 and twin law −*k*, −*h*, and −*l*. The structure was refined using the PHENIX program with the data between 29.46 and 1.8 Å, for which $F \geq 2\sigma(F)$ with alternating cycles of positional- and individual-temperature-factor refinement. Twin refinement was included in the rounds of refinement, resulting in improved maps compared to those without twin refinement. The resulting model was inspected and modified using the COOT program. In the final stages of the refinement, water molecules were added to the model with electron-density acceptance criteria of $F \geq 3\sigma F$ in the *Fo*−*Fc* difference electron-density map. Vanadate and KDO were added to the model in the final round of the refinement. A simulated annealing omit map with coefficients 2*Fo*−*Fc* was calculated by omitting ligands VO_3^- and KDO and running one round of simulated annealing refinement in PHENIX (current composite omit routines cannot account for twinning). The unit-cell parameters, data collection, and refinement statistics are presented in Table 2.

dx.doi.org/10.1021/bi400659k | *Biochemistry* 2013, 52, 5372−5386

Table 1. Steady-State Kinetic Constants Determined for Selected Members of the YbrI Clade As Catalysts of KDN9P and KDO8P Hydrolysis[a]

YbrI-clade phosphatase	substrate	k_{cat} (s^{-1})	K_m (μM)	k_{cat}/K_m (M^{-1} s^{-1})	k_{cat}/K_m ratio[b]	k_{cat} ratio[b]	functional assignment
B. thetaiotaomicron BT1713	KDO8P	0.092 ± 0.003	430 ± 70	2.0×10^2	0.018	0.077	
	KDN9P	1.2 ± 0.1	110 ± 9	1.1×10^4			KDN9PP
S. avermitillis Q82HY3	KDO8P	0.094 ± 0.003	122 ± 8	7.7×10^2	0.64	0.47	
	KDN9P	0.20 ± 0.01	170 ± 10	1.2×10^3			KDN9PP
B. thetaiotaomicron BT1677	KDO8P	1.5 ± 0.3	0.10 ± 0.04	1.5×10^4	217	25	
	KDN9P	0.061 ± 0.005	0.9 ± 0.2	6.9×10^1			KDO8PP
E. coli P0ABZ4	KDO8P	13 ± 1	170 ± 20	7.7×10^5	4500	168	
	KDN9P	0.077 ± 0.004	460 ± 90	1.7×10^2			KDO8PP
H. influenza HI1679	KDO8P	0.78 ± 0.04	160 ± 20	4.8×10^3	370	37	
	KDN9P	0.021 ± 0.003	1600 ± 500	1.3×10^1			KDO8PP
L. pneumophila Q52 × 93	KDO8P	0.080 ± 0.004	46 ± 6	1.7×10^3	94	4.4	
	KDN9P	0.018 ± 0.001	1000 ± 100	1.8×10^1			KDO8PP
P. syringae Q48EB9	KDO8P	0.60 ± 0.04	50 ± 7	1.2×10^4	670	6.7	
	KDN9P	0.017 ± 0.002	960 ± 40	1.8×10^1			KDO8PP
V. cholerae Q9KP52	KDO8P	0.089 ± 0.002	19 ± 2	4.7×10^3	200	3.6	
	KDN9P	0.025 ± 0.001	1100 ± 100	2.3×10^1			KDO8PP

[a]In 50 mM K^+HEPES containing 2 mM $MgCl_2$ (pH 7.0, 25 °C). [b]The ratio reflects the value of the kinetic constant measured using KDO8P as substrate divided by the value of the kinetic constant measured using KDN9P as substrate.

The final model consisted of residues 1−179 (Gln 180 was disordered). KDO was modeled in the active site but in two different orientations: one in which KDO is coordinated to VO_3^- and the other in which KDO C8−OH forms a hydrogen bond to an oxygen atom of VO_3^- (Figure S13).

Structures of the KDN9PP and KDO8PP Orthologs. The X-ray crystallographic structures of the KDO8PPs from *P. syringae*, *L. pneumophila*, and *V. cholera* and KDN9PP from *S. avermitilis* were also determined. The detailed protocols are reported in the Supporting Information, and the specific unit-cell parameters, data collection, and refinement statistics are presented in Table S1.

Determination of the Steady-State Kinetic Constants. The steady-state kinetic constants were measured for BT-KDN9PP (BT1713), BT-KDO8PP (BT1677), Q9KP52 (*Vibrio cholerae*), Q48EB9 (*Pseudomonas syringae*), Q5ZX93 (*Legionella pneumophila subsp. pneumophila*), HI1679 (*Haemophilus influenza*), P0ABZ4 (*Escherichia coli*), and Q82HY3 (*Streptomyces avermitillis*) using a previously published procedure.[9,17]

Bioinformatic Analysis. The list of KDN9PP and KDO8PP sequences were identified by first carrying out BLAST[25] searches of the available bacterial (3919) and archaeal (250) genomes in NCBI and the Genome database. The KDN9PP sequences were confirmed by the presence of the corresponding synthases or additional biological context in the case of the KDO8PP sequences (Supporting Information, Supplemental Results). Highly redundant sequences were removed (>90%), and the remaining sequences were checked for the presence of a complete set of catalytic residues (for example, BT-KDN9PP Asp10, Asp12, Thr54, Lys80, Asp103, and Asp107), indicating catalytic activity. The resultant sequences were curated and sorted using the specificity markers for KDN9PP (Glu56/Lys67 pair) and KDO8PP (either Arg60 based on HI-KDO8PP numbering or Gly63 based on BT-KDO8PP numbering). The KDN9PP and KDO8PP fusion proteins were parsed into separate groups. The accuracy of the sorting of the KDN9PP and KDO8PP sequences was confirmed by examining the co-occurrence of a likely KDN9P synthase or KDO8P synthase gene, respectively. The sequences within the respective groups were aligned using Clustal Omega.[26] The phylogenetic tree was generated using ClustalW2 Phylogenetic Tree Tool[27] and exported in Newick format. The tree of life was generated from iTOL (itol.embl.de)[28] and downloaded in the Newick format. FigTree (http://tree.bio.ed.ac.uk/software/figtree/) was used for visualization and figure generation. The sequence logo figures were generated using WebLogo.[29]

RESULTS AND DISCUSSION

Determination of Substrate Preference. We began the investigation of the divergence of the structure, substrate recognition, and biological function within the HADSF YbrI clade with the KDO8PP and KDN9PP paralogs from *Bacteriodes thetaiotaomicron* (BT1677 and BT1713). Ultimately, we also included KDO8PP and KDN9PP homologues from phylogenetically diverse bacteria. KDN9PP and the KDN biosynthetic pathway (Scheme 1) were first discovered in *B. thetaiotaomicron*.[17] BT1713 was found to catalyze the hydrolysis of KDN9P ($k_{cat}/K_m = 3 \times 10^4$ M^{-1} s^{-1}), *N*-acetylneuraminate 9-phosphate (Neu5Ac-9P, $k_{cat}/K_m = 6 \times 10^3$ M^{-1} s^{-1}), and KDO8P ($k_{cat}/K_m = 2 \times 10^2$ M^{-1} s^{-1}), yet it was found to have little activity toward other phosphate ester metabolites.[9] The gene encoding BT1713 was also found to be adjacent to those of a synthase (BT1714) and KDN−CMP transferase (BT1715).[17] The gene context combined with the substrate specificity analysis led to the identification of BT1713 as BT-KDN9PP. BT1677 was proposed to be BT-KDO8PP, but it had not yet been previously characterized. However, the homologous KDO8PP operative in the KDO pathway (Scheme 1) in *Haemophilus influenza* (HI-KDO8PP)[7] and in *Escherichia coli* (EC-KDO8PP) were known.[8] The presence of the KDO pathway in *B. thetaiotaomicron* was evident from the presence of the complete set of genes associated with the pathway (viz., KDO8P synthase, BT4321; KDO8PP, BT1677; and KDO−CMP transferase, BT0725), which are homologous to the genes of the *E. coli* KDO pathway.

Steady-state kinetic techniques were used to determine the turnover rates (k_{cat}) and the substrate specificity constants (k_{cat}/K_m) for the hydrolysis of KDN9P and KDO8P catalyzed by

dx.doi.org/10.1021/bi400659k | *Biochemistry* 2013, 52, 5372−5386

BT1713, BT1677, and the structurally characterized homologues from *E. coli* (EC)[8] and *H. influenza* (HI).[7] In the end, the homologues from *S. avermitilis* (SA), *P. syringae* (PS), *V. cholera* (VC), and *L. pneumophila pneumophila str. Philadelphia 1* (LP) were included. These homologues were produced in the early stages of the Enzyme Function Initiative for the purpose of structure-based function determination.

With the exception of BT-KDN9PP and the *S. avermitilis* homologue, each of the enzymes showed significantly higher k_{cat} and k_{cat}/K_m values as catalysts of KDO8P hydrolysis than for KDN9P hydrolysis (Table 1). The *E. coli* homologue displayed the highest level of discrimination with the KDO8P/KDN9P k_{cat} ratio equal to 168 and the k_{cat}/K_m ratio equal to 4500, respectively. The KDO8P/KDN9P k_{cat} ratio reflects the ability of the enzyme to orient the bound substrate in a manner that is optimal for catalytic turnover (viz., productive binding). The k_{cat}/K_m ratio, however, reflects both substrate-binding affinity and proper orientation. It follows that the active site of the *E. coli* homologue binds and orients KDO8P much more effectively than it does KDN9P. This specialization is consistent with the biological role of this enzyme as the KDO8PP operative in the *E. coli* KDO biosynthetic pathway.[8]

The KDO8P/KDN9P k_{cat} and k_{cat}/K_m ratios measured for BT1677 and the HI, LP, PS, and VC homologues (k_{cat}/K_m ratio equal to 217, 370, 94, 670, and 200, respectively and k_{cat} ratio equal to 25, 37, 4.4, 6.7, and 3.6, respectively) indicate a broad range in selectivity. It is also evident from these data that the KDO8P binding affinity is the predominate determinant of selectivity. The kinetic constant ratios are consistent with the findings from bioinformatic analysis (vide infra) because each of these enzymes functions in the KDO pathway, as indicated by their co-occurrence with the pathway KDO8P synthase. Thus, hereafter each of these homologues will be referred to as a KDO8PP from a particular source (e.g., BT-KDO8PP). BT1713 and the *S. avermitilis* homologue, however, function in the KDN pathway (vide infra) and thus are named BT-KDN9PP and SA-KDN9PP.

SA-KDN9PP was engineered as a singleton protein from a two-domain protein composed of the KDN9PP domain and the KDN−CMP-transferase domain. The comparatively lower k_{cat}/K_m values (7.7×10^2 and 1.2×10^3 M^{-1} s^{-1} for KDO8P and KDN9P, respectively) observed for SA-KDN9PP might be the consequence of this engineering. Nevertheless, KDN9P is the preferred substrate. BT-KDN9PP, however, displays a catalytic efficiency toward its physiological substrate that is similar to the catalytic efficiencies of the KDO8PP enzymes toward KDO8P. Moreover, BT-KDN9PP prefers KDN9P over KDO8P by a significant factor (KDN9P/KDO8P k_{cat} and k_{cat}/K_m ratios of 13 and 56, respectively).

In light of these differences in specificity, we turned to structural information to uncover the binding determinants. The structure of BT-KDN9PP liganded to *N*-acetylneuraminate (Neu5Ac) is available[9] but not the complex with KDN. The KDO-liganded structure of *E. coli* KDO8PP has been described,[16] but because of the resolution there is some ambiguity as to the identity of the substrate-binding residues. Although this work is informative, it does not assist in elucidating the basis of the specificity and functional divergence or in clearly demarcating these paralogous enzymes. To identify differences in the active-site structure that might account for the observed substrate selectivity, the X-ray crystallographic structures of these KDOPP and KDN9PP orthologs were determined alone and in complex with transition-state analogs.

Table 2. Data Collection and Refinement Statistics for BT-KDO8PP Bound with Mg^{2+}, BT-KDN9PP Bound with Mg^{2+}, VO_3^-, and KDN, and HI-KDO8PP Bound with Mg^{2+}, KDO, and VO_3^-[a]

data collection	BT-KDO8PP-Mg^{2+}	BT-KDN9PP-Mg^{2+}-VO_3^--KDN	HI-KDO8PP-Mg^{2+}-VO_3^--KDO
PDB ID	4HGN	4HGO	4HGP
space group	$P2_12_12_1$	$P2_12_12$	$I4$
cell dimension (Å)	a = 37.52	a = 81.30	a = b = 79.85
	b = 91.20	b = 106.32	c = 52.15
	c = 170.07	c = 74.15	
molecules/ASU	4	4	1
wavelength (Å)	1	1.54	1.54
resolution (Å)	85.1 − 1.8 (1.86 − 1.8)	28.5 − 2.1 (2.2 − 2.1)	29.5 − 1.8 (1.89 − 1.8)
observed reflections	261 122	220 160	120 635
unique reflections	50 327	38 011	14 537
completeness (%)	91.1 (79.7)	95.5 (99.0)	95.6 (91.4)
R_{sym} (%)[b]	6.1 (43.2)	7.6 (48.3)	5.73 (38.13)
$\langle I/\sigma \rangle$	19.6 (2.79)	6.29 (2.5)	13.68 (2.40)
redundancy	5.3 (4.7)	5.4 (2.73)	7.9 (5.7)
twin law			$-k, -h, -l$
twin fraction			0.33
Refinement			
R/R_{free}	17.56/21.83	19.02/24.71	14.73/16.52
no. of atoms			
protein/water	5064/329	5143/176	1352/177
Mg^{2+}/VO_3^--KDO or VO_3^--KDN	8/NA	4/52	1/36
average temperature factor (Å^2)			
protein/water	23.3/28.6	22.5/23.1	18.3/26.0
Mg^{2+}/VO_3^--KDO or VO_3^--KDN	24.2/NA	24.5/36.5	15.4/20.5
Ramachandran statistics			
favored/allowed/outlier (%)	98/2/0	96.6/3.4/0	96/2/0
rms deviation from ideal			
bonds	0.008	0.010	0.011
angles	1.094	1.082	1.184
clash score	8.74	12.00	10.44

[a]Values in parentheses are for the highest-resolution shell. NA indicates not applicable. [b]$R_{sym} = \sum_{hkl} \sum_i |I_{hkl,\,i} - \langle I_{hkl} \rangle I| / \sum_{hkl} \sum_i |I_{hkl,\,i}|$, where $\langle I_{hkl} \rangle$ is the mean intensity of the multiple $I_{hkl,\,i}$ observations for symmetry-related reflections.

X-ray Crystal Structures of Mg^{2+} and Mg^{2+}/Metavanadate-Sugar Acid Complexes of KDN9PP and KDO8PP. The X-ray crystal structures of KDN9PP and KDO8PP bound to Mg^{2+} (the cofactor) alone or to the complex of Mg^{2+}, metavanadate (VO_3^-), and the corresponding sugar acid (KDO or KDN) were determined (Figure S1). Our initial goal was to determine the structures of BT-KDN9PP bound to KDN and KDO and the structures of BT-KDO8PP bound to KDO and KDN. However, we were only successful in obtaining the structures of the BT-KDN9PP-Mg^{2+}-VO_3^--KDN complex and BT-KDO8PP bound to Mg^{2+} (Table 2). For the representation of the liganded KDO8PP complex, we determined the structure of HI-KDO8PP-Mg^{2+}-VO_3^--KDO (Table 2) but, unfortunately, not the corresponding KDN complex. Finally, the structures of SA-KDN9PP-Ca^{2+}, PS-KDO8PP-Mg^{2+}, VC-

dx.doi.org/10.1021/bi400659k | *Biochemistry* 2013, 52, 5372−5386

KDO8PP-Mg^{2+}, and LP-KDO8PP-Ca^{2+} were determined (Table S1).

Comparison of the Structures of the BT-KDN9PP-Mg^{2+}-VO_3^--KDN9PP and HI-KDO8PP-Mg^{2+}-VO_3^--KDO Complexes. A representative dimer (encompassing one active site) from each of the tetrameric structures of liganded BT-KDN9PP and HI-KDO8PP is shown in Figures 2A and 3A, respectively. Mg^{2+} and VO_3^- are coordinated by the residues of the catalytic subunit, and KDN and KDO are bound by residues of the cap and catalytic subunits. Figures 2B and 3B highlight the catalytic residues, whereas Figures 2C and 3C highlight the KDN- and KDO-binding residues, respectively.

The BT-KDN9PP-Mg^{2+}-VO_3^--KDN9P and HI-KDO8PP-Mg^{2+}-VO_3^--KDO structures (Figures 2B and 3B) provide snapshots that represent the transition state for the first step of the two-step phosphoryl transfer reaction. In this step, the Asp nucleophile attacks the substrate phosphoryl group displacing, with the assistance of the Asp acid, acid sugar KDN or KDO (Scheme 2). The vanadium assumes a five-coordinate, trigonal bipyramidal coordination geometry, in which the three oxygen atoms from the metavanadate are located in equatorial positions, and the Asp nucleophile carboxylate group (BT-KDN9PP Asp10 and HI-KDO8PP Asp14) and the KDN C9−O or KDO C8−O are located at the apical positions, suggestive of a backside, in-line displacement of the substrate leaving group during catalytic turnover. The carboxylate groups of the respective Asp acid catalysts (BT-KDN9PP Asp12 and HI-KDO8PP Asp16) are engaged in hydrogen-bond formation with KDN C9−O or KDO C8−O. Motif 2 Thr/Ser and motif 3 Lys (BT-KDN9PP Thr54 and Lys80 and HI-KDO8PP Ser58 and Lys84) form hydrogen bonds with the two of equatorial oxygen atoms, and Mg^{2+} forms a coordination bond to the third equatorial oxygen atom. Mg^{2+} is also coordinated to the non-reacting oxygen atom of the Asp nucleophile carboxylate group, the backbone carbonyl oxygen atom of the Asp acid, one of the two oxygen atoms of the metal-binding motif 4 Asp/Glu residues (BT-KDN9PP Asp103 and HI-KDO8PP Asp107), and two water molecules.

The residues that bind the substrate leaving group (KDN or KDO) via hydrogen-bond formation (Figures 2C and 3C) are of special interest because they are expected to play important roles in the discrimination between KDN9P and KDO8P. The KDN moiety bound to BT-KDN9PP is anchored by a hydrogen bond with Glu56, which is located on the catalytic subunit, and with Arg64, Lys67, and Thr34 located on the cap subunit. A hydrogen-bond network is formed between Glu56 and KDN C(7)OH, C(2)OH, and cap-subunit Lys67, which in turn forms a hydrogen bond with KDN C(2)OH. Arg64 forms two hydrogen bonds with the KDN carboxylate group, and Thr34 forms hydrogen bonds with KDN C(6)O and C(7)OH. KDN C(4)OH and C(5)OH do not form hydrogen bonds with the enzyme but are instead solvent exposed. The same orientation was observed for the Neu5Ac-9P ligand in the previously reported structure of the BT-KDN9PP-Mg^{2+}-VO_3^--Neu5Ac complex (Figure S2).[9]

The structure of the HI-KDO8PP-Mg^{2+}-VO_3^--KDO complex (Figure 3C) indicates that the KDO moiety of the KDO8P substrate engages in hydrogen-bond formation with cap subunit residues Arg68 (salt bridge between the side chain and both oxygen atoms of the KDO carboxylate), Val38 (backbone C═O and KDO C(2)OH), Leu42 (backbone NH and KDO C(2)OH), and Met178 (backbone C═O and KDO C(3)OH) and with the catalytic subunit residue Arg60 (hydrogen bond between the side chain and a KDO carboxylate group oxygen atom).

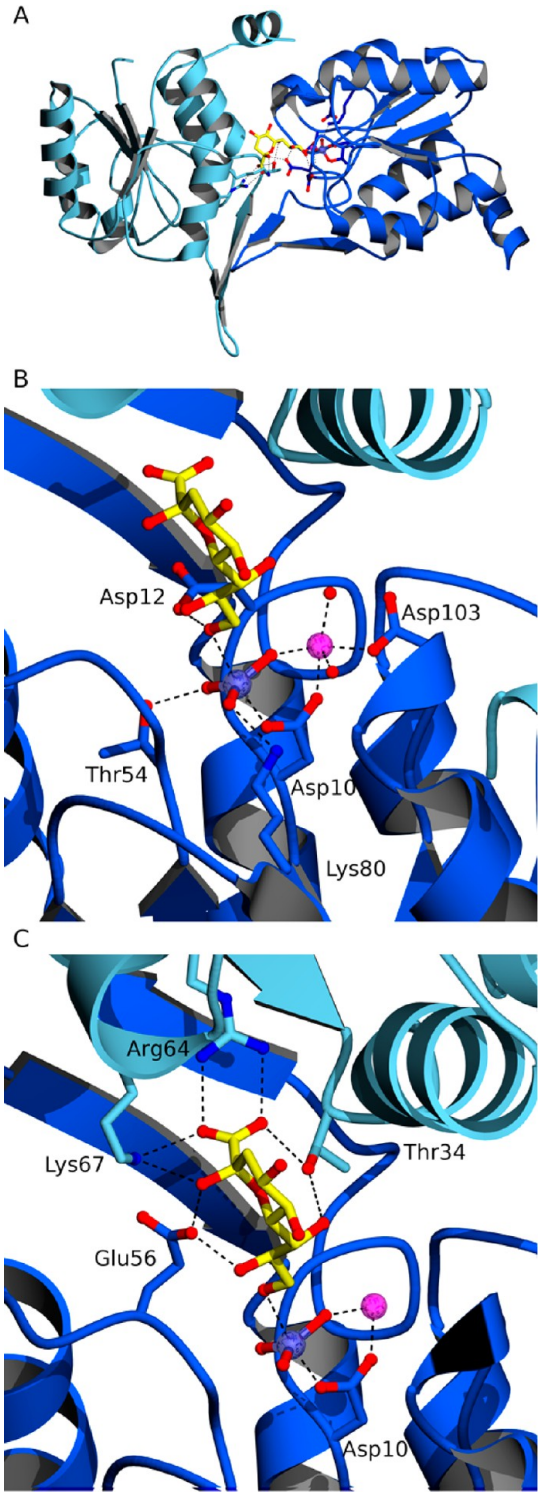

Figure 2. Structure of BT-KDN9PP-Mg^{2+}-VO_3^--KDN. (A) Dimer from tetrameric BT-KDN9PP. The catalytic subunit is colored dark blue, and the cap subunit, light blue. The HAD catalytic motifs are shown as dark-blue sticks, and KDN, as yellow sticks. Vanadium is colored slate blue, and magnesium is a magenta sphere. (B) HAD catalytic residues and (C) KDN-binding residues. Panels B and C are colored the same as in panel A.

The hydrogen bonds between the KDN moiety and the BT-KDN9PP active-site residues indicate that Glu56, Arg64, Lys67,

dx.doi.org/10.1021/bi400659k | Biochemistry 2013, 52, 5372−5386

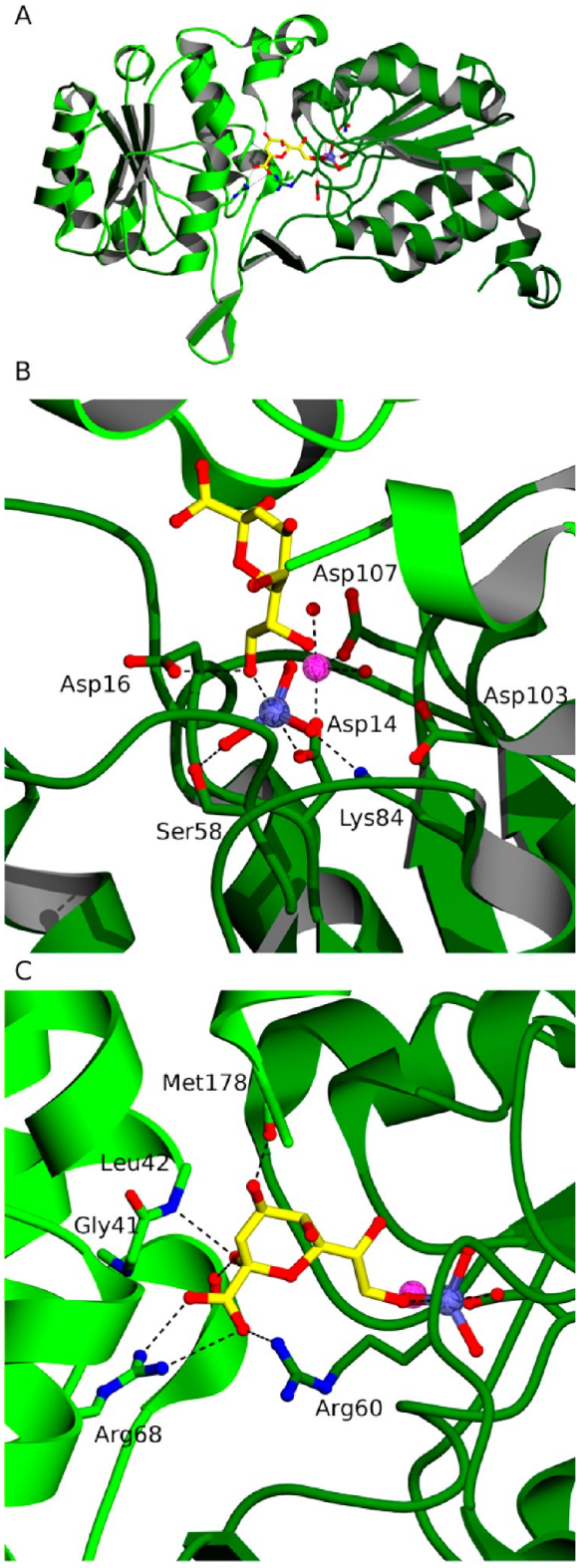

Figure 3. Structure of HI-KDO8PP-Mg^{2+}-VO_3^--KDO. (A) Dimer of HI-KDO8PP (generated from symmetry mates comprising tetramer). The catalytic subunit is colored forest green, and the cap subunit, light green. The HAD catalytic motifs are shown as forest-green sticks, and KDN, as yellow sticks. Vanadium is colored slate blue, and magnesium is a magenta sphere. (B) HAD catalytic residues and (C) KDN-binding residues. Panels B and C are colored the same as in panel A.

and Thr34 are key KDN-binding residues. Likewise, the hydrogen bonds formed between KDO and the HI-KDO8PP active-site residues suggest Arg68 and Arg60 (plus Val38, Leu42, and Met178 that bind via their backbone amide groups) are the key KDO-binding residues. To determine if these two sets of residues are conserved in KDN9PP and KDO8PP homologues, the X-ray structures of BT-KDN9PP and SA-KDN9PP were compared to the X-rays structures of HI-, PS-, VC-, and LP-KDO8PP determined in the present work as well as that of the EC-KDO8PP previously reported.[16]

Comparison of the KDN- and KDO-Binding Residues among Structurally Characterized KDN9PP and KDO8PP Enzymes. *KDN9PP Enzymes.* BT-KDN9PP and SA-KDN9PP originate from evolutionarily distant bacterial species that belong to two separate phyla (Bacteroidetes and Actinobacteria, respectively). BT-KDN9PP is a standalone protein, whereas SA-KDN9PP is one catalytic domain within a two-domain fusion protein that includes the KDN−CMP transferase. BT-KDN9PP and SA-KDN9PP possess 31% sequence identity and have similar tertiary and quaternary structures (Figure S3). The superposition of the BT-KDN9PP-Mg^{2+}-VO_3^--KDN and SA-KDN9PP-Ca^{2+} structures (Figure S4) reveals some degree of divergence in the catalytic site (viz., BT-KDN9PP Thr54 and Asp103 are replaced by Ser62 and Asn110 in SA-KDN9PP) and in the KDN binding site (BT-KDN9PP residue Thr34 is replaced with Arg42). However, BT-KDN9PP Glu56, Arg64, and Lys67 are conserved in SA-KDN9PP as Glu64, Arg72 and Lys75, respectively. A sequence alignment of the single-domain KDN9PP proteins and the KDN9PP-KDN−CMP transferase fusion proteins shows that all three of these binding residues are stringently conserved (vide infra).

KDO8PP Enzymes. HI-KDO8PP and BT-KDO8PP also originate from evolutionarily divergent bacterial species (HI belongs to the phylum Proteobacteria). These two orthologs share only 24% sequence identity, yet they have similar tertiary and quaternary structures (Figure S5). The superposition of the structure of the HI-KDO8PP-Mg^{2+}-VO_3^--KDO complex with the structure of the BT-KDO8PP-Mg^{2+} complex shows that the catalytic residues are largely conserved (BTKDO8PP Asp 17, Asp19, Thr58, Lys87, and Asp110 vs HI-KDO8PP Asp14, Asp16, Ser58, Lys84, and Asp107), whereas the KDO-binding residues are not as well conserved (Figure 4). The HI-KDO8PP cap-subunit residues Val38 and Leu42 correspond to Ile41 and Tyr45 in BT-KDO8PP. However, the positions of the backbone amide groups of BT-KDO8PP Ile41 and Tyr45 are similar to those of HI-KDO8PP Val38 and Leu42; therefore, it is likely that the two hydrogen bonds formed to the KDO moiety are conserved despite the fact that the amino acid side chains are not. The counterpart to the HI-KDO8PP cap subunit Arg68 is Arg71 and thus this salt bridge interaction is retained. In contrast, the hydrogen bond between the HI-KDO8PP catalytic subunit Arg60 side chain and the KDO carboxylate group has no counterpart in BT-KDO8PP (Figure 4). BT-KDO8PP Gly63 is located at the HI-KDO8PP Arg60 position; although Arg64 is next in the sequence, it is not in position for salt-bridge formation with the KDO carboxylate group (Figure 4). In addition, the hydrogen bond to KDO C(4)OH formed by the HI-KDO8PP cap-domain residue Asn48 (side chain) is altered or lost in BT-KDO8PP because of the replacement of Asn48 with Lys45 (Figure S5). Because the C-terminus of BT-KDO8PP could not be modeled in the X-ray crystallographic structure, a seven-residue truncation of BT-KDO8PP (BT-KDO8PP Δ167) was generated to ascertain

dx.doi.org/10.1021/bi400659k | *Biochemistry* 2013, 52, 5372−5386

Scheme 2. Chemical Pathway Catalyzed by the HADSF Phosphatase

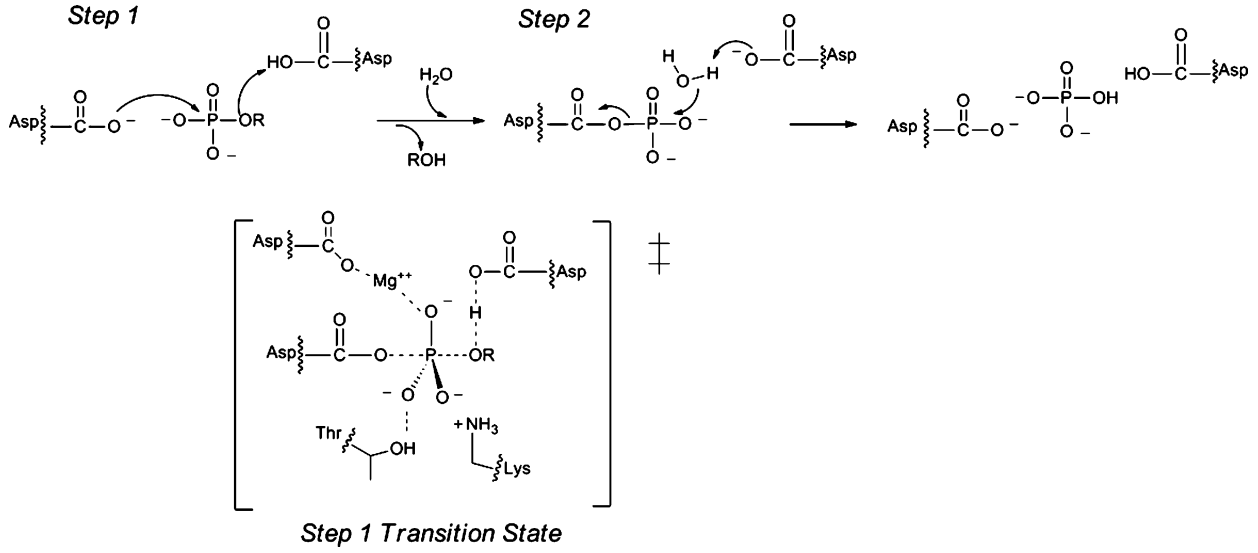

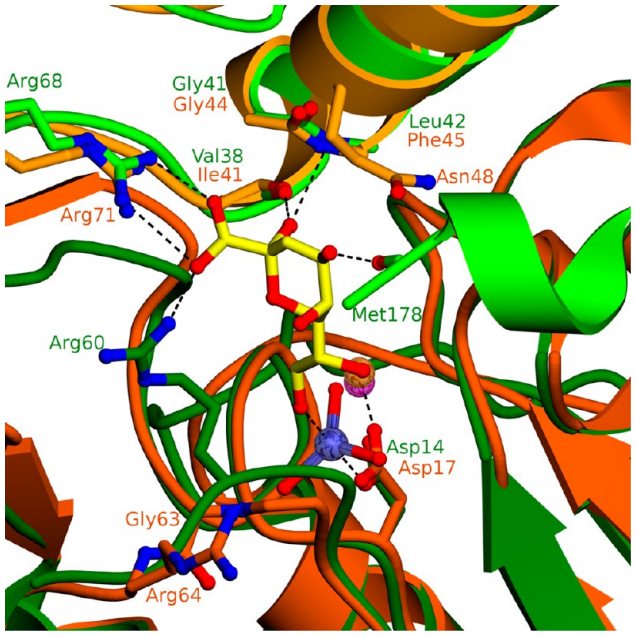

Figure 4. Overlay of the HI-KDO8PP and BT-KDO8PP active sites. The dimer of HI-KDO8PP (generated from symmetry mates comprising tetramer) with its catalytic subunit colored forest green, and cap subunit, light green. KDN is shown as yellow sticks, vanadium is colored slate blue, and magnesium is a magenta sphere. The dimer of BT-KDO8PP with its catalytic subunit colored dark orange, and cap subunit, light orange. Magnesium is an orange sphere. The putative substrate-binding residues are shown as sticks and labeled in their corresponding enzyme color. Hydrogen bonds and coordination bonds are shown as dashed lines.

whether the BT-KDO8PP C-terminus plays an analogous role to that of the HI-KDO8PP C-terminus (where there is a hydrogen bond between KDO C(4)OH and the Met178 C═O). BT-KDO8PP Δ167 was found to have a k_{cat} of 0.10 s^{-1} and k_{cat}/K_m of 1.3 × 10^4 M^{-1} s^{-1}, which is 15- and 115-fold lower than that of full length BT-KDO8PP, indicating the C-terminus of BT-KDO8PP plays a role in catalysis or substrate positioning.

The superposition of the structures of HI-, BT-, PS-, LP-, EC-, and VC-KDO8PP (Figure S6) shows that VC-KDO8PP and PS-KDO8PP are similar to HI-KDO8PP in that they conserve the position of the catalytic subunit Arg60 as Arg75 and Arg69, respectively. Thus, they are likely to use these residues, along with their respective cap-subunit residues Arg83 and Arg77, to bind the KDO carboxylate group. EC-KDO8PP Arg78 (homologous to HI-KDO8PP Arg60) is not correctly oriented for interaction with the KDO carboxylate group in this structure, but because of the flexible nature of the Arg side chain, it can be modeled in the productive position. LP-KDO8PP, however, is unique in that Ala71 rather than a Gly (Gly63 in BT-KDO8PP) corresponds to HI-KDO8PP Arg60, and Gln72 corresponds to BT-KDO8PP Arg64. It is anticipated that neither LP-KDO8PP Ala71 or Gln72 contribute to binding KDO.

Although the overall sequence divergence among these six KDO8PPs is quite high (25−58% pairwise sequence identity; Table S2), the backbone fold is highly conserved such that it is likely that the hydrogen bonds formed between KDO and the HI-KDO8PP backbone Val38 C═O and Leu42 NH have counterparts in BT-, PS-, LP-, EC-, and VC-KDO8PP (Figure S6).

One can observe a distinct classification of KDO sequences by their specificity residues (Arg vs Gly) by analyzing the alignment of orthologous sequences (Figures S7 and S8). This suggests an evolutionary divergence along more than one pathway (vide infra). The only KDO-binding residue that is stringently conserved in KDO8PP is the cap-subunit Arg (HI-HDO8PP Arg68, BT-KDO8PP Arg71, etc.), which is also stringently conserved among the KDN9PPs (Figure S9).

KDN Versus KDO Orientation. The superposition of the structures of the BT-KDN9PP-Mg^{2+}-VO_3^--KDN and HI-KDO8PP-Mg^{2+}-VO_3^--KDO complexes (Figure S10) indicates that KDO8PP binds the alpha epimer of KDO, whereas KDN9PP binds the beta epimer of KDN. Although the respective ring carboxylate groups are similarly positioned to form salt bridges with the KDO8PP and KDN9PP cap-domain Arg side chains, the KDN and KDO C(2)OH groups are oriented toward the opposite sides of the respective binding sites. Specifically, KDN C(2)OH is proximal to BT-KDN9PP cap-subunit Lys67 and catalytic subunit Glu56 with which it

dx.doi.org/10.1021/bi400659k | *Biochemistry* 2013, 52, 5372−5386

Table 3. Comparison of Wild-Type and Mutant BT-KDN9PP and BT-KDO8PP Steady-State Kinetic Constants Measured for the Catalyzed Hydrolysis of KDN9P and KDO8P[a]

enzyme	substrate	k_{cat} (s^{-1})	K_m (mM)	k_{cat}/K_m (M^{-1} s^{-1})	k_{cat}/K_m ratio[b]
BT-KDO8PP WT	KDO8P	1.5 ± 0.3	0.10 ± 0.04	1.5×10^4	217
	KDN9P	0.061 ± 0.005	0.9 ± 0.2	69	
BT-KDO8PP Δ167	KDO8P	0.10 ± 0.1	0.76 ± 0.01	1.3×10^2	
BT-KDN9PP WT	KDO8P	0.092 ± 0.003	0.43 ± 0.07	2×10^2	0.018
	KDN9P	1.2 ± 0.1	0.105 ± 0.009	1.1×10^4	
BT-KDN9PP E56A	KDO8P	0.109 ± 0.02	0.207 ± 0.09	5×10^2	8.3
	KDN9P	0.026 ± 0.002	0.41 ± 0.01	6×10^1	
BT-KDN9PP E56A/K67A	KDO8P	0.062 ± 0.002	0.196 ± 0.009	3.1×10^2	75
	KDN9P	0.004 ± 0.0008	0.99 ± 0.03	4.1	

[a]In 50 mM K^+HEPES containing 2 mM $MgCl_2$ (pH 7.0, 25 °C). [b]The ratio reflects the value of the kinetic constant measured using KDO8P as substrate divided by the value of the kinetic constant measured using KDN9P as substrate.

forms hydrogen bonds. KDO C(2)OH, however, is oriented toward the KDO8PP cap-subunit (α-helix) backbone Val38 C═O and Leu42 NH with which it forms hydrogen bonds. Given that KDO8P is a slow substrate for BT-KDN9PP and KDN9P is a slow substrate for KDO8PP, it would be of interest to know if the alternate substrate binds the ring in the same orientation as the natural substrate. However, attempts to obtain the X-ray structures of the corresponding complexes were unsuccessful.

Substrate Specificity and Structure of Glu56Ala and Glu56Ala/Lys67Ala BT-KDN9PP. Common to each of the KDN9PP and KDO8PP enzymes examined is the potential for salt-bridge formation between the KDO or KDN carboxylate group and the cap-subunit Arg residue (BT-KDN9PP Arg64, HI-KDO8PP Arg68, etc.). Ala replacement of this Arg in BT-KDN9PP removes all detectable activity.[9] Sequence alignments (Figures S7−9) indicate that this Arg residue is invariant. Therefore, the Arg is considered to be a key substrate-binding residue in both KDN9PP and KDO8PP. Each of the KDO8PPs tested (Table 1) show catalytic activity with KDN9P that is significantly less than that observed with KDO8P. A Glu-Lys pair (BT-KDN9PP Glu56-Lys67) formed by a Glu that originates from the catalytic subunit and a Lys from the cap subunit appear to play a key role in the divergence of KD9PP function. These Glu and Lys residues make hydrogen bonds with KDN C(2)OH, and the Lys also forms a salt bridge with the KDN carboxylate residue. In BT-KDO8PP, the corresponding residues are Gly63 and Ala74.

If the BT-KDN9PP Glu56-Lys67 residues were replaced with Ala residues, then would the substrate selectivity change? To address this question, the BT-KDN9PP Glu56Ala variant was prepared as well as the Glu56Ala/Lys67Ala variant (the Lys67Ala variant proved to be insoluble). The X-ray crystallographic structures of Glu56Ala and Glu56Ala/Lys67Ala BT-KDN9PP proteins were determined (Table S3) to verify their retention of the native fold. Neither structure differs significantly from that of wild-type BT-KDN9PP, with rmsd values of 0.2 and 0.3 Å for the Glu56Ala and Glu56Ala/Lys67Ala variants, respectively. With the exception of the mutation site, the active sites were unchanged (Figure S11).

The steady-state kinetic constants were measured for the catalysis of KDN9P or KDO8P hydrolysis by the single and double mutant (Table 3). Compared to wild-type with KDN9P serving as substrate, the Glu56Ala mutant displayed a 46-fold decrease in k_{cat} and a 180-fold decrease in k_{cat}/K_m, whereas the Glu56Ala/Lys67Ala mutant displayed a 300-fold decrease in k_{cat} and a 2700-fold decrease in k_{cat}/K_m. Thus, both residues make a significant contribution to the substrate-binding affinity and orientation. In contrast, with KDO8P serving as substrate the k_{cat} and k_{cat}/K_m values are essentially unchanged by the mutations. These results suggest that when bound to the KDN9PP active site KDO8P does not engage in hydrogen-bond formation with the Glu56-Lys67 pair. Indeed, if KDO8P were to bind to KDN9PP in the same ring orientation as that observed for KDO in the HI-KDO8PP-Mg^{2+}-VO_3^--KDO structure (vide supra), then hydrogen-bond formation between KDO C(2)OH and the Glu56-Lys67 pair would not be possible.

Bioinformatic Analysis of KDO8PP and KDN9PP Evolution. A bioinformatic study of KDO8PP and KDN9PP was carried out in which the genes encoding the KDO8PP and KDN9PP orthologs in all available bacterial (3919) and archaeal (250) genomes in the NCBI public data bank were identified, and the encoded protein sequences were analyzed within the context of multiple sequence alignments. (See the Materials and Methods section for details.) The purpose of this analysis was 3-fold: (1) to define the variation in the identities of the key active-site residues revealed by the X-ray crystallographic structures, (2) to examine the evolutionary distance between the orthologs, and (3) to map the biological ranges of the KDO8PP and KDN9PP orthologs within the boundaries set by the sequence represented in NCBI.

Identification of Separate Categories of KDO8PP and KDN9PP Orthologs and Analysis of Their Distribution. Of the total 1380 nonredundant ortholog sequences identified, 1246 were found to be KDO8PPs and 134 were found to be KDN9PPs (46 KDN9PP genes and 88 genes encoding a fusion protein composed of a KDN9PP domain and a KDN−CMP transferase domain; Table 4). The cap-subunit substrate-binding Arg residue (BT-KDN9PP Arg64, HI-KDO8PP Arg68, and BT-KDO8PP Arg71; Figures 2C, 3C, and 4) is present in all sequences. The alignment of the 987 KDO8PP orthologs (Table 4) that are distinguished by the KDO8P-binding Arg located at the catalytic subunit (HI-KDO8PP Arg60; Figure 3C) is represented by the sequence logo shown in Figure S7. There is a group of KDO8PP ortholog sequences found in Fusobacteria (26 total) in which this residue is replaced by a Lys (Table 4 and the sequence logo shown in Figure S7). It is assumed that the Lys side chain can substitute for the Arg side chain in salt-bridge formation with the KDO carboxylate group. The alignment of the 259 KDO8PP sequences that possesses a Gly (or in a smaller number of sequences, Ala) (BT-KDO8PP Gly63; Figure 4) in place of Arg is represented by the sequence logo shown in Figure S8. The

dx.doi.org/10.1021/bi400659k | Biochemistry 2013, 52, 5372−5386

Table 4. Summary of the Bioinformatic Results[a]

source	genes identified	KDO8PP	KDN9PP
Archaea	3	0	2
			1 fusion
Acidobacteria	11	7 Arg	3
		1 Gly	
Actinobacteria	51	0	51 fusion
Aquificae	10	10 Arg	0
Bacteroides	244	10 Arg	18
		200 Gly	16 fusion
Chlorobi	14	0	14
Chloroflexi	1		1 fusion
Chrysiogenetes	1	1Arg	0
Cyanobacteria	15	1 Arg	0
		14 Gly	
Deferibacteres	4	4 Arg	0
Elusomicrobia	2	1 Arg	0
		1 Gly	
Firmicutes/Bacilli	4	4 Arg	0
Firmicutes/Clostridia	26	18 Arg, 1 Arg fusion	7 fusion
Firmicutes/ Negativicutes	47	46 Arg	1
Fusobacteria	28	26 Lys[b]	0
		2 Ala[c]	
Gemmatimonadetes	1	1Arg	0
Lentisphaera	1	1 Arg	0
Proteobacteria/Alpha	7	1 Arg	2
			4 fusion
Proteobacteria/Beta	189	182 Arg, 6 Arg fusion	1 fusion
Proteobacteria/Delta	48	36 Arg, 3 Arg fusion	1
		6 Gly	2 fusion
Proteobacteria/Epsilon	59	54Arg	4
			1 fusion
Proteobacteria/Gamma	556	529 Arg, 8 Arg fusion	0
		19 Gly	
Proteobacteria/Zeta	1	1 Arg	0
Nitrospirae	6	4 Arg, 1 Arg fusion	1
Planctomycetes	13	12 Arg	1 fusion
Spirochaetes	18	8 Ser[d], 8 Asn[e]	2 fusion
Synergistetes	11	11 Arg	0
Thermodesulfobacteria	3	3 Arg	0
Verrucomicrobia	6	5 Arg	1

[a]Column 1 lists the taxonomic rank of the source of the KDN9PP and/or KDO8PP encoding genes, column 2 lists the number of genes found within that source, and columns 3 and 4 specify the distribution according to assigned protein identity (see the text for details). [b]Lys replaces the catalytic subunit Arg-specificity residue (HI-KDO8PP Arg60). [c]Ala replaces the catalytic subunit Gly of the KDO8PP-Gly lineage (BT-KDO8PP Gly63). [d]Ser replaces the catalytic subunit Gly of the KDO8PP-Arg lineage (HI-KDO8PP Arg60). [e]Asn replaces the catalytic subunit Gly of the KDO8PP-Arg lineage (HI-KDO8PP Arg60).

Spirochaetes phyla contains 16 KDO8PP sequences with Asn (8 total) or Ser (8 total) in place of the Arg residue; these have been excluded from the sequence logo figures. The alignment of the KDN9PP ortholog sequences (represented by the sequence logo of Figure S9) illustrates the conserved (catalytic subunit) Glu-Lys (cap subunit) KDN9P-specific binding motif (BT-KDN9PP Glu56-Lys67; Figure 2C).

A quantitative analysis of the sequences that comprise the different categories of KDO8PP (KDO8PP-Arg (fusion vs singleton), KDO8PP-Lys, KDO8PP-Ser, KDO8PP-Asn, and KDO8PP-Gly/Ala) and KDN9PP (fusion vs singleton) orthologs among the various phyla or divisions is reported in Table 4. Figure 5A provides a schematic of the distribution of KDN9PP and KDO8PP orthologs among bacterial phyla in the form of a 16S rRNA-rooted phylogenetic tree. A detailed description of the biological distribution of the KDO8PP and KDN9PP orthologs in relation to the occurrence of lipopolysaccharide (LPS) synthesis is provided in the Supporting Information.

The occurrence of the KDO8PP orthologs is directly coupled with the occurrence of LPS (such as lipid A of Proteobacteria) of which KDO is a common component. LPSs function at the outer membrane surface of diderm (gram-negative) bacteria. Diderms comprise the majority of bacterial phyla.[30] The number of KDN9PP orthologs is comparatively smaller than the number of KDO8PP orthologs, which suggests that KDN is used for a more specialized biological function than that of KDO-containing LPS.

Although KDO8PP orthologs are broadly distributed among diderms but not monoderms (gram-positive bacteria), KDN9PP orthologs are selectively distributed among both. For example, KDO8PP orthologs were not found in Archaea, Chlorobi (diderm), and Acintobacteria (monoderm), whereas 3, 14, and 51 KDN9PP orthologs were found therein, respectively. In contrast, we found 845 KDO8PP orthologs in Proteobacteria as compared to 15 KDN9PP orthologs. Likewise, 28 KDO8PP orthologs were found in Fusobacteria and 15 in Cyanobacteria, whereas no KD9PP orthologs were found therein. In Bacteroides (the closest relative of Chlorobi), 34 KDN9PP orthologs were detected compared to 210 KDO8PP orthologs.

The biological function of KDN appears to be host-dependent. Actinobacteria is a monoderm whose cytoplasmic membrane is elaborated with anionic cell-wall polymers (teichuronic acid) containing KDN.[31−35] However, certain symbiotic Bacteroides species are thought to use KDN in capsular polysaccharides that are displayed on the outer membrane for the purpose of host mimicry.[17,36]

Notably, there were several examples of bacteria wherein a KDN9PP ortholog appears to substitute for a bona fide KDO8PP ortholog in KDO synthesis. Specifically, the Chlorobi phyla includes diderms having outer membrane LPS that contains KDO.[37] Bioinformatic analysis identified 12 KDN9PP orthologs as well as 13 KDO8PP-Arg orthologs. The 13 KDO8PP-Arg orthologs lack the essential Asp nucleophile and thus are assumed to be catalytically inert. Therefore, in these species, the KD9PP orthologs must be functioning in the KDO pathway. In addition, we found four species within epsilonproteobacteria that possess KDN9PP orthologs (*Helicobacter bizzozeronii* CCUG 35545, *Helicobacter bizzozeronii* CIII, *Helicobacter felis* ATCC 49179, and *Helicobacter heilmannii* ASB1.4). These species do not possess a KDO8PP gene but do possess both KDN9P and KDO8P synthase genes. Finally, we note that whereas KDO is present in the LPS[38−40] of alphaproteobacteria, only one of the seven genes identified in these organisms encode a KDO8PP ortholog and the remaining genes encode a KDN9PP ortholog.

Evolutionary Distance Between KDO8PP and KDN9PP Orthologs. The evolutionary distance between the different categories of KDO8PP and KDN9PP orthologs is represented in Figure 5B in the form of an unrooted phylogenetic tree generated using the alignment of all KDO8PP and KDN9PP

dx.doi.org/10.1021/bi400659k | *Biochemistry* 2013, 52, 5372−5386

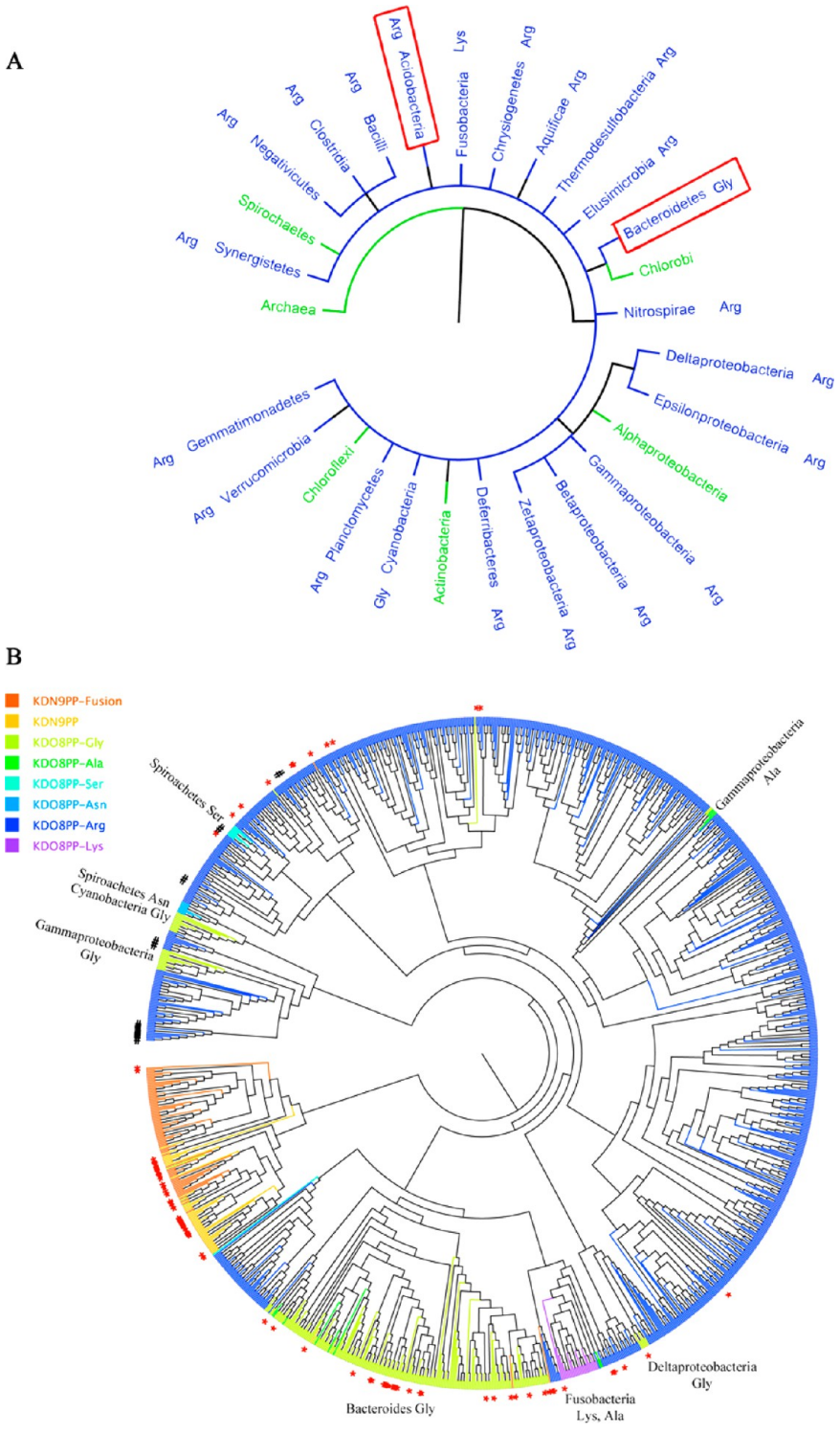

Figure 5. Schematics of Bioinformatic Analyses. (A) Tree of life generated from iTOL (itol.embl.de) displaying phyla (and class in the case of proteobacteria) that contain KDO8PP and KDN9PP sequences. Phyla are color-coded (KDO8PP blue and KDN9PP green) on the basis of the majority presence of enzymes. Red boxes indicate the two phyla that contain species with both KDN9PP and KDO8PP. The type of KDO8PP enzyme (Arg, Lys, or Gly) is indicated next to the phyla name. (B) Unrooted phylogenetic tree generated using a multiple-sequence alignment of all KDO8PP and KDN9PP enzymes identified herein. KDO8PP-Arg enzymes are colored blue, KDO8PP-Gly, green, KDN9PP, light orange, and KDN9PP-KDN−CMP transferase fusions, deep orange. Red stars indicate enzymes that were identified where an additional KDN9PP or KDO8PP gene exists within the species. Black symbols (#) indicate KDO8PP-Arg-KDO−CMP transferase fusion genes. The phyla of some KDO8PP-Gly enzymes have been labeled. This figure was generated with FigTree (http://tree.bio.ed.ac.uk/software/figtree/).

sequences identified herein. Because the sequences that comprise the KDO8PP-Arg category greatly outnumber the rest, the tree appears to be rooted in KDO8PP-Arg; no significance is attributed to this point. Rather, we focus on the pattern observed in the grouping of the sequences from the different categories because this indicates the structural

dx.doi.org/10.1021/bi400659k | *Biochemistry* 2013, 52, 5372−5386

relatedness between these sequences, which in turn reflects shared versus independent paths in evolution.

From the inspection of Figure 5B, it is clear that the KDN9PP sequences (light orange) and the KDN9PP-KDN−CMP transferase fusion-protein sequences (deep orange) group together and separate from the KDO8PP sequences (dark blue, cyan, and green). The conservation of the Lys-Glu substrate-specificity motif among all KDN9PP and KDN9PP-KDN−CMP transferase fusion-protein sequences indicates a single lineage for the bacterial KDN pathway phosphatase, which has spread across phyla in a rather species-selective manner.

It is also evident from the examination of Figure 5B that two major lineages of KDO8PP orthologs have evolved: one with the catalytic subunit Arg functioning as the substrate-specificity residue and the other distinguished by the replacement of this Arg by Gly, as the two categories of sequences group separately. The KDO8PP orthologs from Fusobacteria, which possess Lys (26 sequences) and Ala (2 sequences) at the specificity position, group with the KDO8PP-Arg category sequences. The KDO8PP-Gly lineage is concentrated in Bacteroides (200 KDO8PP-Gly orthologs vs 10 KDO8PP-Arg orthologs), whereas the KDO8PP-Arg lineage is concentrated in Proteobacteria (820 KDO8PP-Arg orthologs vs 25 KDO8PP-Gly orthologs). Finally, we note that the KDO8PP-CMP−KDO fusion proteins (indicated with a black # symbol in Figure 5B) were specifically formed from the KDO8PP-Arg orthologs.

The few KDO8PP-Arg orthologs that appear in Bacteroides are more closely related in sequence to the Proteobacteria KDO8PP-Arg orthologs than they are to the Bacteroides KDO8PP-Gly orthologs, suggestive of horizontal gene transfer. In contrast, the KDO8PP-Gly orthologs that are found outside of Bacteroides (e.g., in gammaproteobacteria and Cyanobacteria) are more closely related in sequence to the KDO8PP-Arg orthologs than they are to the Bacteroides KDO8PP-Gly orthologs. In addition, Spiroachetes contains KDO8PP-Asn and -Ser orthologs that cluster with KDO8PP-Arg orthologs, indicating that there is some relaxation in the selection pressure to maintain Arg at the specificity position.

CONCLUSIONS

The KDO8PP orthologs are the products of specialization within the C0 class of HADSF phosphatases, which are involved in the incorporation of a sequence insert to serve as an oligomerization motif for tetramer formation. The interfaced subunits provide the catalytic scaffold and the substrate-binding residues in a division of tasks. The vast majority of HADSF phosphatases belong to the C1 or C2 class and thus employ a cap-domain insertion in the Rossmann-fold catalytic scaffold to function in substrate selection. The C0 HADSF phosphatases were the first to evolve,[4] and now they comprise a comparatively small class of this superfamily.

KDO8PP and KDN9PP orthologs display phosphatase activity toward both substrates, although a significantly greater activity was observed with the physiological substrate. We attribute the substrate promiscuity to a stringently conserved cap-subunit Arg residue, which forms a salt bridge with the carboxylate substituent common to both substrates. The X-ray crystallographic structural data indicate that KDN9PP and KDO8PP bind different epimers of their physiological substrates. The KDN9PP orthologs conserve a Glu-Lys motif that functions in KDN9P binding via the carboxylate and C(2)OH groups. Removal of this motif in BT-KDN9PP by replacement with Ala greatly diminished its activity toward KDN9P but not KDO8P. Thus, the Glu-Lys motif, which is absent in the KDO8PP orthologs, seems to be the product of selection for enhanced activity toward KDN9P and the branch point for the KDN9PP lineage from that of the KDO8PP. The retention of significant KDN9PP activity toward KDO8P provides the opportunity for substitution of KDN9PP for KDO8PP as the phosphatase of the KDO pathway.

The KDO8PP orthologs augment the salt bridge between the cap-subunit Arg and the KDO9P carboxylate group, with hydrogen bonds formed between three backbone amide groups and the substrate ring hydroxyl substituents. The largest lineage of KDO8PP orthologs (KDO8PP-Arg) employ an Arg residue in the catalytic subunit to form a second salt bridge to the substrate carboxylate group. The other lineage, KDO8PP-Gly, evolved separately and does not include the catalytic subunit Arg, but rather a Gly or in some instances Ala is located at the Arg position. Within specific phyla or genera of bacteria, variants of the KDO8PP-Arg lineage are found that have undergone what we speculate to be subsequent conservative amino-acid replacement at the Arg site (viz., Lys in Fusobacteria) or nonconservative amino-acid replacement (viz., Gly in cyanobacteria and Ser in Spirochaetes). Taken together, the KDO8PP and KDN9PP orthologs of the class C0 YrbI clade display a diversity in substrate-recognition elements that underlie a range in substrate promiscuity and in turn changeability in biological function.

ASSOCIATED CONTENT

Supporting Information

Additional methods; KDN9PP and KDO8PP orthologs data collection and refinement statistics; pair-wise sequence identities between the KDO8PP and KDN9PP sequences that have been subjected to X-ray structure determination; BT-KDN9PP mutant data collection and refinement statistics; quaternary structures of BT-KDN9PP-Mg^{2+}-$VO3^{-}$-KDN, HI-KDO8PP-Mg^{2+}-$VO3^{-}$-KDO, and BT-KDO8PP-Mg^{2+}; superposition of the structure of BT-KDN9PP bound with Mg^{2+}, *N*-acetylneuramic acid, and metavanadate with the structure of BT-KDN9PP bound with Mg^{2+}, KDN, and metavanadate; SA-KDN9PP-Ca^{2+} tetramer; superposition of the BT-KD9PP-Mg^{2+}-$VO3^{-}$-KDN and SA-KDN9PP-Ca^{2+} structures zoomed in on the KDN-binding residues; superposition of the HI-KDO8PP-Mg^{2+}-$VO3^{-}$-KDO and BT-KDO8PP-Mg^{2+} tetramers showing two of the four subunits; overlay of the HI, BT, PS, LP, EC, and VC-KDO8PP active sites; sequence logos generated from multiple sequence alignments of all KDO8PP sequences with either Arg or Gly at the specificity position; sequence logo generated from a multiple sequence alignment of all KDN9PP sequences; overlay of the HI-KDO8PP-Mg-VO3-KDO and BT-KDN9PP-Mg-VO3-KDN active sites; BT-KDN9PP mutant structures; and stereo views of the 2Fo-Fc composite-omit and simulated-annealing electron density maps. This material is available free of charge via the Internet at http://pubs.acs.org.

Accession Codes

The coordinates of E56A, E56A/K67A, and KDNPP complexed with 2-keto-3-deoxynononate and metavanadate from *B. thetaiotaomicron*, KDO8PP from *B. thetaiotaomicron*, and KDO8PP complexed with 2-keto-3-deoxy-D-manno-octulosonate and metavanadate from *H. influenzae* have been deposited in the Protein Data Bank under accession codes 4HGQ, 4HGR, 4HGO, 4HGN, and 4HGP.The coordinates of the phosphatase orthologs from *S. avermittillis*, *P. syringae*, *V.*

cholera, and *L. pneumophila* have been deposited in the Protein Data Bank under accession codes 3MMZ, 3MN1, 3N07, and 3N1U, respectively.

AUTHOR INFORMATION

Corresponding Author

*E-mail: dd39@unm.edu; Tel: (505) 277-3383; Fax: (505) 277-6202 (D. D.-M.). E-mail: drkallen@bu.edu; Tel (617)-358-5544; Fax: (617) 353-6466 (K. N. A.).

Present Address

[#]Center for Integrative Proteomics Research, Department of Chemistry and Chemical Biology, Rutgers, The State University of New Jersey, Piscataway, NJ 08854, United States.

Funding

This work was supported by National Institutes of Health U54 GM093342 (to K.N.A., D.D.-M., and S.C.A). The NYSGXRC was supported by NIH grant U54 GM074945 (to S.K.B.).

Notes

The authors declare no competing financial interest.

ACKNOWLEDGMENTS

We gratefully acknowledge the efforts of all NYSGXRC personnel who contributed to the structure determination. The Center for Synchrotron Biosciences, where the diffraction data were collected, was supported by grant P30-EB-009998 from the National Institute of Biomedical Imaging and Bioengineering (NIBIB). Use of the National Synchrotron Light Source, Brookhaven National Laboratory, was supported by the U.S. Department of Energy, Office of Science, Office of Basic Energy Sciences, under contract no. DE-AC02-98CH10886.

ABBREVIATIONS

BT, *Bacteroides thetaiotaomicron*; EC, *Escherichia coli*; HADSF, Haloalkanoate dehalogenase superfamily; HI, *Haemophilus influenzae*; LP, *Legionella pneumophila*; KDO, 2-keto-3-deoxy-D-manno-octulosonate; KDO8P, 2-keto-3-deoxy-D-manno-octulosonate 8-phosphate; KDO8PP, 2-keto-3-deoxy-D-manno-octulosonate-8-phosphate phosphatase; KDN, 2-keto-3-deoxynononate; KDN9P, 2-keto-3-deoxynononate 9-phosphate; KDN9PP, 2-keto-3-deoxynononate-9-phosphate phosphatase; LPS, lipopolyscaccharide; Neu5Ac, *N*-acetylneuraminate; Neu5Ac-9P, *N*-acetylneuraminate 9-phosphate; PS, *Pseudomonas syringae*; SA, *Streptomyces avermitilis*; VC, *Vibrio cholera*

REFERENCES

(1) Nguyen, H. H., Wang, L., Huang, H., Peisach, E., Dunaway-Mariano, D., and Allen, K. N. (2010) Structural determinants of substrate recognition in the HAD superfamily member D-glycero-D-manno-heptose-1,7-bisphosphate phosphatase (GmhB). *Biochemistry 49*, 1082−1092.

(2) Huang, H., Patskovsky, Y., Toro, R., Farelli, J. D., Pandya, C., Almo, S. C., Allen, K. N., and Dunaway-Mariano, D. (2011) Divergence of structure and function in the haloacid dehalogenase enzyme superfamily: bacteroides thetaiotaomicron BT2127 is an inorganic pyrophosphatase. *Biochemistry 50*, 8937−8949.

(3) Rangarajan, E. S., Proteau, A., Wagner, J., Hung, M. N., Matte, A., and Cygler, M. (2006) Structural snapshots of *Escherichia coli* histidinol phosphate phosphatase along the reaction pathway. *J. Biol. Chem. 281*, 37930−37941.

(4) Burroughs, A. M., Allen, K. N., Dunaway-Mariano, D., and Aravind, L. (2006) Evolutionary genomics of the HAD superfamily: understanding the structural adaptations and catalytic diversity in a superfamily of phosphoesterases and allied enzymes. *J. Mol. Biol. 361*, 1003−1034.

(5) Allen, K. N., and Dunaway-Mariano, D. (2009) Markers of fitness in a successful enzyme superfamily. *Curr. Opin. Struct. Biol. 19*, 658−665.

(6) Selengut, J. D. (2001) MDP-1 is a new and distinct member of the haloacid dehalogenase family of aspartate-dependent phosphohydrolases. *Biochemistry 40*, 12704−12711.

(7) Parsons, J. F., Lim, K., Tempczyk, A., Krajewski, W., Eisenstein, E., and Herzberg, O. (2002) From structure to function: YrbI from *Haemophilus influenzae* (HI1679) is a phosphatase. *Proteins 46*, 393−404.

(8) Wu, J., and Woodard, R. W. (2003) *Escherichia coli* YrbI is 3-deoxy-D-manno-octulosonate 8-phosphate phosphatase. *J. Biol. Chem. 278*, 18117−18123.

(9) Lu, Z., Wang, L., Dunaway-Mariano, D., and Allen, K. N. (2009) Structure-function analysis of 2-keto-3-deoxy-D-glycero-D-galactonononate-9-phosphate phosphatase defines specificity elements in type C0 haloalkanoate dehalogenase family members. *J. Biol. Chem. 284*, 1224−1233.

(10) Onishi, H. R., Pelak, B. A., Gerckens, L. S., Silver, L. L., Kahan, F. M., Chen, M. H., Patchett, A. A., Galloway, S. M., Hyland, S. A., Anderson, M. S., and Raetz, C. R. (1996) Antibacterial agents that inhibit lipid A biosynthesis. *Science 274*, 980−982.

(11) Strohmaier, H., Remler, P., Renner, W., and Hogenauer, G. (1995) Expression of genes kdsA and kdsB involved in 3-deoxy-D-manno-octulosonic acid metabolism and biosynthesis of enterobacterial lipopolysaccharide is growth phase regulated primarily at the transcriptional level in *Escherichia coli* K-12. *J. Bacteriol. 177*, 4488−4500.

(12) Belunis, C. J., Clementz, T., Carty, S. M., and Raetz, C. R. (1995) Inhibition of lipopolysaccharide biosynthesis and cell growth following inactivation of the kdtA gene in *Escherichia coli*. *J. Biol. Chem. 270*, 27646−27652.

(13) Cipolla, L., Polissi, A., Airoldi, C., Galliani, P., Sperandeo, P., and Nicotra, F. (2009) The Kdo biosynthetic pathway toward OM biogenesis as target in antibacterial drug design and development. *Curr. Drug Discovery Technol. 6*, 19−33.

(14) Cipolla, L., Polissi, A., Airoldi, C., Gabrielli, L., Merlo, S., and Nicotra, F. (2011) New targets for antibacterial design: Kdo biosynthesis and LPS machinery transport to the cell surface. *Curr. Med. Chem. 18*, 830−852.

(15) Inoue, S., Kitajima, K., and Inoue, Y. (1996) Identification of 2-keto-3-deoxy-D-glycero−galactonononic acid (KDN, deaminoneuraminic acid) residues in mammalian tissues and human lung carcinoma cells. Chemical evidence of the occurrence of KDN glycoconjugates in mammals. *J. Biol. Chem. 271*, 24341−24344.

(16) Biswas, T., Yi, L., Aggarwal, P., Wu, J., Rubin, J. R., Stuckey, J. A., Woodard, R. W., and Tsodikov, O. V. (2009) The tail of KdsC: conformational changes control the activity of a haloacid dehalogenase superfamily phosphatase. *J. Biol. Chem. 284*, 30594−30603.

(17) Wang, L., Lu, Z., Allen, K. N., Mariano, P. S., and Dunaway-Mariano, D. (2008) Human symbiont *Bacteroides thetaiotaomicron* synthesizes 2-keto-3-deoxy-D-glycero-D-galacto-nononic acid (KDN). *Chem. Biol. 15*, 893−897.

(18) Otwinowski, Z., and Minor, W. (1997) Processing of X-ray diffraction data collected in oscillation mode. *Methods Enzymol. 276*, 307−326.

(19) Vagin, A., and Teplyakov, A. (2010) Molecular replacement with MOLREP. *Acta Crystallogr., Sect. D 66*, 22−25.

(20) Potterton, E., Briggs, P., Turkenburg, M., and Dodson, E. (2003) A graphical user interface to the CCP4 program suite. *Acta Crystallogr., Sect. D 59*, 1131−1137.

(21) Winn, M. D. (2003) An overview of the CCP4 project in protein crystallography: an example of a collaborative project. *J. Synchrotron Radiat. 10*, 23−25.

(22) Adams, P. D., Afonine, P. V., Bunkoczi, G., Chen, V. B., Davis, I. W., Echols, N., Headd, J. J., Hung, L. W., Kapral, G. J., Grosse-Kunstleve, R. W., McCoy, A. J., Moriarty, N. W., Oeffner, R., Read, R.

J., Richardson, D. C., Richardson, J. S., Terwilliger, T. C., and Zwart, P. H. (2010) PHENIX: a comprehensive Python-based system for macromolecular structure solution. *Acta Crystallogr., Sect. D 66*, 213−221.
(23) Emsley, P., and Cowtan, K. (2004) Coot: model-building tools for molecular graphics. *Acta Crystallogr., Sect. D 60*, 2126−2132.
(24) (2007) *PROTEUM2, Version 2.4*, Bruker AXS, Inc., Madison, Wisconsin.
(25) McGinnis, S., and Madden, T. L. (2004) BLAST: at the core of a powerful and diverse set of sequence analysis tools. *Nucleic Acids Res. 32*, W20−25.
(26) Sievers, F., Wilm, A., Dineen, D., Gibson, T. J., Karplus, K., Li, W., Lopez, R., McWilliam, H., Remmert, M., Soding, J., Thompson, J. D., and Higgins, D. G. (2011) Fast, scalable generation of high-quality protein multiple sequence alignments using Clustal Omega. *Mol. Syst. Biol. 7*, 539.
(27) Larkin, M. A., Blackshields, G., Brown, N. P., Chenna, R., McGettigan, P. A., McWilliam, H., Valentin, F., Wallace, I. M., Wilm, A., Lopez, R., Thompson, J. D., Gibson, T. J., and Higgins, D. G. (2007) Clustal W and Clustal X version 2.0. *Bioinformatics 23*, 2947−2948.
(28) Letunic, I., and Bork, P. (2011) Interactive Tree Of Life v2: online annotation and display of phylogenetic trees made easy. *Nucleic Acids Res. 39*, W475−478.
(29) Crooks, G. E., Hon, G., Chandonia, J. M., and Brenner, S. E. (2004) WebLogo: a sequence logo generator. *Genome Res. 14*, 1188−1190.
(30) Sutcliffe, I. C. (2010) A phylum level perspective on bacterial cell envelope architecture. *Trends Microbiol. 18*, 464−470.
(31) Shashkov, A. S., Tul'skaya, E. M., Evtushenko, L. I., Denisenko, V. A., Ivanyuk, V. G., Stomakhin, A. A., Naumova, I. B., and Stackebrandt, E. (2002) Cell wall anionic polymers of Streptomyces sp. MB-8, the causative agent of potato scab. *Carbohydr. Res. 337*, 2255−2261.
(32) Shashkov, A. S., Kosmachevskaya, L. N., Streshinskaya, G. M., Evtushenko, L. I., Bueva, O. V., Denisenko, V. A., Naumova, I. B., and Stackebrandt, E. (2002) A polymer with a backbone of 3-deoxy-D-glycero-D-galacto-non-2-ulopyranosonic acid, a teichuronic acid, and a beta-glucosylated ribitol teichoic acid in the cell wall of plant pathogenic Streptomyces sp. VKM Ac-2124. *Eur. J. Biochem. 269*, 6020−6025.
(33) Tul'skaia, E. M., Shashkov, A. S., Bueva, O. V., and Evtushenko, L. I. (2007) [Anionic carbohydrate-containing cell wall polymers of Streptomyces melanosporofaciens and related species]. *Mikrobiologiia 76*, 48−54.
(34) Naumova, I. B., and Shashkov, A. S. (1997) Anionic polymers in cell walls of gram-positive bacteria. *Biochemistry (Moscow) 62*, 809−840.
(35) Tul'skaya, E. M., Shashkov, A. S., Streshinskaya, G. M., Senchenkova, S. N., Potekhina, N. V., Kozlova, Y. I., and Evtushenko, L. I. (2011) Teichuronic and teichulosonic acids of actinomycetes. *Biochemistry (Moscow) 76*, 736−744.
(36) Xu, J., Mahowald, M. A., Ley, R. E., Lozupone, C. A., Hamady, M., Martens, E. C., Henrissat, B., Coutinho, P. M., Minx, P., Latreille, P., Cordum, H., Van Brunt, A., Kim, K., Fulton, R. S., Fulton, L. A., Clifton, S. W., Wilson, R. K., Knight, R. D., and Gordon, J. I. (2007) Evolution of symbiotic bacteria in the distal human intestine. *PLoS Biol. 5*, e156.
(37) Meißner, J., Fischer, U., and Weckesser, J. (1987) The lipopolysaccharide of the green sulfur bacterium *Chlorobium vibrioforme f. thiosulfatophilum*. *Arch. Microbiol. 149*, 125−129.
(38) Forsberg, L. S., Bhat, U. R., and Carlson, R. W. (2000) Structural characterization of the O-antigenic polysaccharide of the lipopolysaccharide from *Rhizobium etli* strain CE3. A unique O-acetylated glycan of discrete size, containing 3-O-methyl-6-deoxy-L-talose and 2,3,4-tri-O-,methyl-l fucose. *J. Biol. Chem. 275*, 18851−18863.
(39) Forsberg, L. S., and Carlson, R. W. (1998) The structures of the lipopolysaccharides from *Rhizobium etli* strains CE358 and CE359. The complete structure of the core region of *R. etli* lipopolysaccharides. *J. Biol. Chem. 273*, 2747−2757.
(40) Forsberg, L. S., and Carlson, R. W. (2008) Structural characterization of the primary O-antigenic polysaccharide of the *Rhizobium leguminosarum* 3841 lipopolysaccharide and identification of a new 3-acetimidoylamino-3-deoxyhexuronic acid glycosyl component: a unique O-methylated glycan of uniform size, containing 6-deoxy-3-O-methyl-D-talose, n-acetylquinovosamine, and rhizoaminuronic acid (3-acetimidoylamino-3-deoxy-D-gluco-hexuronic acid). *J. Biol. Chem. 283*, 16037−16050.
(41) Kraulis, P. (1991) MOLSCRIPT: a program to produce both detailed and schematic plots of protein structures. *J. Appl. Crystallogr. 24*, 946−950.
(42) Fenn, T. D., Ringe, D., and Petsko, G. A. (2003) POVScript+: a program for model and data visualization using persistence of vision ray-tracing. *J. Appl. Crystallogr. 36*, 944−947.